IEEE Access
Multidisciplinary ⋮ Rapid Review ⋮ Open Access Journal

Received 21 March 2024, accepted 28 May 2024, date of publication 5 June 2024, date of current version 13 June 2024.

Digital Object Identifier 10.1109/ACCESS.2024.3409936

RESEARCH ARTICLE

Near-Field Phased Array Diagnostics by a Subspace Projection Method

MARIA ANTONIA MAISTO[1], (Member, IEEE), MARIO DEL PRETE[1], (Student Member, IEEE), ANTONIO CUCCARO[2], AND RAFFAELE SOLIMENE[1,3], (Senior Member, IEEE)

[1]Department of Engineering, University of Campania "Luigi Vanvitelli," Aversa, 81031 Caserta, Italy
[2]Department of Informatics, Modeling, Electronics and Systems Engineering (DIMES), University of Calabria, 87036 Rende, Italy
[3]Department of Electrical Engineering, Indian Institute of Technology Madras, Chennai 600036, India

Corresponding author: Mario Del Prete (mario.delprete@unicampania.it)

This work was supported in part by Italian Ministry of Research (MUR) through the Progetti di Rilevante Interesse Nazionale [Projects of Relevant National Interest (PRIN)] Project PLasma Advanced Sensing Methodologies And Reconstructions in Ecr ion sources (PLASMARE) under Grant 2022YSW5R5, and in part by the PRIN-Piano nazionale di ripresa e resilienza [National Recovery and Resilience Plan (PNRR)] Project Non-invasive millimetrIc electroMagnetic imAging from phasEless measuRement of multI-layered mAterials (NIMAERIA) under Grant P2022PS843.

ABSTRACT This paper aims to introduce a new strategy for the detection of faulty elements in phased array antennas. The approach takes advantage on the possibility in phased array to introduce the steering diversity. Accordingly, by collecting the radiated field over the measurement aperture while steering the beam, an approach inspired by the Time reversal MUSIC (TR-MUSIC) algorithm is exploited to achieve the diagnostics. At first, it is shown that such an algorithm allows the detection of only completely turned-off elements as long as the number of defective elements is relatively (depending on the configuration parameters) high. To overcome such a limitation, the difference model is built and the approach succeeds in detecting any failure (amplitude and phase failure) by a reduced set of data, mainly depending on the number of faulty elements. In addition, from the mere knowledge of the geometric parameters of the measurement configuration and by invoking the theory of degrees of freedom, the conditions for which the algorithm succeeded in the diagnostics are analytically derived. Furthermore, it is highlighted that the proposed algorithm achieves the diagnostics even when both the spacing between the array elements and the element factor is not a priori known. An extensive Montecarlo numerical analysis is included to show the capability of the approach to achieve a high probability of detection with a reduced set of data. Finally, full-wave simulations are also included.

INDEX TERMS Array diagnostics, near field measurements, phased array, TR-MUSIC algorithm.

I. INTRODUCTION

Diagnosing array antennas is a classical and important problem which is necessary to determine if the antenna under test (AUT) complies with the design specifications. This can be accomplished by measuring/estimating the radiation pattern by direct far-field measurements or by near-field to far-field transformations. If the pattern is found to be different with respect to the expected one, then the next step is to discover why this happened and take some action that allows to restore the pattern behavior [1], [2]. To this end, defective elements, that is the array elements whose excitation coefficients deviate from the nominal ones, need to be found out. This requires dealing with an inverse problem where from field measurements the element excitation coefficients, or some quantity related to them, have to be determined. The problem is usually cast as a linear inversion one because the elements' positions are assumed known. If this is not the case, linearity can be maintained by considering the elements' positions as a subset of a much finer search grid. Under the linear framework, the most common and classical methods for addressing diagnostics are by far the so-called back-transformation method (BTM) [3] and the matrix method (MM) [4]. The BTM relies on the field plane-wave spectrum representation and employs the fast Fourier transformation (FFT) algorithm

The associate editor coordinating the review of this manuscript and approving it for publication was Qi Luo.

to back-propagate the measured field at the array aperture. This method is generally limited to planar arrays. The MM basically performs the diagnostics by inverting the corresponding matrix model and hence is more flexible and can handle arrays of general shapes. Methods based on the MUltiple SIgnal Classification (MUSIC) [5] algorithm have been proposed as well. While these methods can in principle only deal with completely turned-off elements, they allow to beat the resolution which is achievable by the BTM and the MM. This is an important feature since isolated defective elements can be easily detected. Instead, due to the limited resolution of classical methods, isolated defective elements tend to be masked by the reconstruction of correctly functioning elements that are adjacent to the fault.

However, the rank deficiency of the data correlation matrix needs to be properly accounted for, otherwise, the performance is no better than BTM or MM. A rank recovery procedure is indeed mandatory. Unfortunately, decorrelation algorithms do not work for near-field configurations. This drawback has been overcome in [6], by spatially employing Fourier transformed field data. Depending on the array's size, the number of required data to achieve diagnostics through the mentioned methods can be very large. Though more advanced sampling methods [7], [8] allow for a great reduction of such a number (as compared to the standard half the wavelength sampling) it can still be too high to achieve quick diagnostics. The number of data can be dramatically reduced by changing perspective and straightway looking for the defective elements, instead of the ones that work correctly. This requires to know/estimate in advance the field radiated by the array without faults (reference array) so that a difference model, with the defective elements as unknowns, can be built. Since the faults are, hopefully, a small fraction of the array elements, the unknown turns out to be sparse. Hence, compressive sensing (CS) algorithms can be conveniently employed to pursue the diagnostics [9], [10], [11]. Many contributions have shown that excellent diagnostic results can actually be achieved with a number of data at least twice as large as the number of faults and that, in principle, it grows only linearly with the number of faults [9]. In particular, CS has proven to work well also for near-field configurations, where the restricted isometry properties are not necessarily guaranteed to hold, even by sampling the data according to the random or the deterministic rules suggested in literature. Moreover, non-convex formulations [12] as well as new mathematical settings based on Lebesgue space of varying exponent [13] have been successfully explored.

The CS has been successfully employed even in the framework of phaseless data [14]. There, the addressed non-linear problem is cast as a convex minimization thanks to the difference model and the low perturbation (to the reference field) due to the small number of faults.

Typically, measurements are collected at different spatial positions. However, phased arrays are usually checked by steering the beam. This opens the possibility to employ data collected while the beam steers in place or in conjunction to the spatial data. Indeed, this idea was already exploited in [15] where the steering diversity is combined with some CS based algorithms. By this strategy, the so-called sensing matrix has the structure of a discrete Fourier transform (DFT) for which most of CS theoretical findings apply. Indeed, the excitation coefficients can be more generally chosen so as to optimize the property of the sensing matrix (for CS purposes) [9]. However, for a practical phased array using digital phase shifters, the range of achievable scanning directions is limited and the scanning states are discrete [15]. Therefore, exploiting the steering diversity in place of the spatial one can lead to a number of independent data insufficient to detect all failures, especially when they affect both the amplitude and phase of the element. Nevertheless, steering the beam (*steering diversity*) is much more convenient since for phased arrays it is already on the table. Also, collecting data through the steering diversity meets the requirement of quick diagnostics.

Therefore, in this paper, the phase domain sampling is combined with the spatial one by taking into account that to speed up the diagnostic procedure one should mainly reduce spatial data without affecting fault detection performance. In particular, the aim is to expand the realm of algorithms for obtaining quick and reliable array diagnostics by exploiting steering diversity. To this end, we reconsider the MUSIC algorithm. More in detail, collecting the radiated field over the measurement aperture while steering the beam leads to a data matrix which enjoys a factorization similar to the so-called multistatic data matrix used in time-reversal MUSIC (TR-MUSIC) [16], [17] for point-like target imaging. Basically, here, the role played by the view diversity in imaging problems is instead due to the steering diversity. Accordingly, a TR-MUSIC based algorithm can be applied to achieve array diagnostics as well. This approach allows us to maintain the super-resolution feature of the MUSIC while avoiding the need for a decorrelation stage. Moreover, the number of required data is much lower than in [6], since the spatial Fourier transformation step is no longer necessary. Indeed, theoretically, the TR-MUSIC works as long as the number of spatial data and steering angles both exceed the number of targets.

The TR-MUSIC can be applied to look for the working elements or the defective ones; in the latter case, the difference model is employed.

In the first case, the TR-MUSIC is convenient for faults represented by completely turned-off elements. Of course, the achievable performance is limited (as for any other method) when the number of properly functioning elements exceeds the number of degrees of freedom of the problem (NDF) (which in turn depends on the measurement configuration) [18]. Nonetheless, when the number of faults is such that the elements in the array do not exceed the NDF, the TR-MUSIC shows amazing detection performances, much better than other methods. In this regard, it can be considered as being

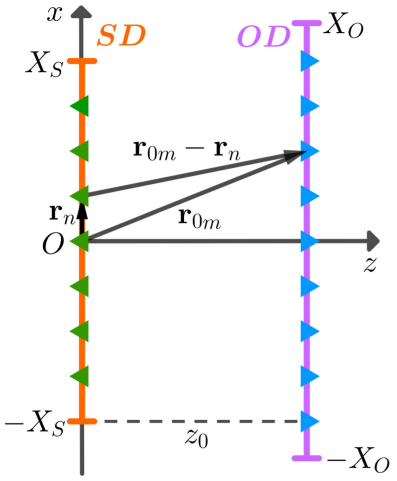

FIGURE 1. Geometry of the problem.

complementary to diagnostic methods that are tailored to deal with sparse unknowns.

When the fault-free reference array is assumed known, the difference model can be considered. Accordingly, the case of few faults can be safely addressed with a reduced set of data. Indeed, say N_D the faults in the array, then the number of required data grows with N_D spatial measurement $\times$ N_D steering angles. Preliminary results of this approach are shown in [19], [20]. Compared to these papers, here, a theoretical discussion is included to derive the conditions ensuring the correct diagnosis in terms of degrees of freedom and, hence, in terms of the measurement configuration parameters. Full-wave simulations are provided to show the capability of the proposed strategy to outperform CS when the element factor of the array is not a priori known. Moreover, TR-MUSIC can also deal well with the case of non-uniform arrays or when the element positions are not known in advance. Finally, while in principle TR-MUSIC allows for the detection of only completely turned-off elements when the difference model is introduced, faults of any type can be detected. The paper is organized as follows. Section II is devoted to giving a mathematical description of the problem. In Section III the TR-MUSIC is detailed whereas Section IV introduces the difference model and discusses the role of the element factor. Section V reports an extensive numerical analysis to validate our approach, whereas Section VI compares our proposed algorithm with CS. Finally, the conclusions end the paper

II. ARRAY DIAGNOSTICS FORMULATION AND BACKGROUND

Consider a linear phased array with N elements deployed over the array aperture $SD = [-X_s, X_s]$. Denote by $\mathbf{r}_n = (x_n, 0)$ the positions of the array elements. The radiated field is collected at M spatial points, $\mathbf{r}_{0m} = (x_{0m}, z_0)$, over the finite linear measurement domain $OD = [-X_0, X_0]$ parallel to SD and located in near-field (with respect to the array) at a distance $z_0 > \lambda$, λ being the wavelength. A schematic view of the radiation problem considered is given in Fig. 1. Note that the array elements, as well as the spatial measurement positions, do not need to be uniform. Therefore, the following discussion applies to uniform and nonuniform arrays.

The radiated field can be written as

$$\underline{E}(\mathbf{r}_{0m}) = \sum_{n=1}^{N} \underline{G}(\mathbf{r}_{0m}, \mathbf{r}_n) c_n \tag{1}$$

where $\underline{E}$ is the vector electric field, $k = 2\pi/\lambda$ is the wavenumber, c_ns are the excitation coefficients, and

$$\underline{G}(\mathbf{r}_{0m}, \mathbf{r}_n) = \frac{e^{-jk|\mathbf{r}_{0m} - \mathbf{r}_n|}}{|\mathbf{r}_{0m} - \mathbf{r}_n|} \underline{f}(\mathbf{r}_{0m}, \mathbf{r}_n) \tag{2}$$

with $\underline{f}(\mathbf{r}_{0m}, \mathbf{r}_n)$ being the element factor.

It is assumed that only one tangent field component is collected. Accordingly, (1) changes and becomes the scalar relationship

$$E_t(\mathbf{r}_{0m}) = \sum_{n=1}^{N} G_t(\mathbf{r}_{0m}, \mathbf{r}_n) c_n \tag{3}$$

where $E_t(\mathbf{r}_{0m})$ denotes one among the x or y field components and $G_t(\mathbf{r}_{0m}, \mathbf{r}_n)$ embodies the corresponding component, $f_t(\mathbf{r}_{0m}, \mathbf{r}_n)$, of the element factor.

Equation (3) can be conveniently arranged in matrix form as

$$\mathbf{e} = \mathbf{G}\,\mathbf{c} \tag{4}$$

where $\mathbf{e} \in C^{M\times 1}$ is the numerical column vector of the electric field (of one of the tangent components indeed) collected over the M measurement positions, $\mathbf{G} \in C^{M\times N}$ is the propagator matrix whose n m entry is given by $G_{nm} = G_t(\mathbf{r}_{0m}, \mathbf{r}_n)$ and $\mathbf{c} \in C^{N\times 1}$ is the coefficient column.

Assume that the array does not comply with the design specification because N_D elements out of N are defective (faulty elements), that is deviate from the nominal ones because of amplitude and/or phase errors. The array diagnostics problem amounts to finding out which elements are defective from field measurements and can be cast as the inversion of (4) for the coefficient vector $\mathbf{c}$.

Let us focus on the particular case where the defective elements are completely turned off. Then, the inversion of (4) in principle allows one to determine the elements that are functioning properly so that the rest of the elements in the array are considered to be faulty.

The BTM and the MM are classical approaches to achieve diagnostics. However, the achievable resolution is limited by the measurement aperture and the distance from the array under test [18]. For example, when considering a measurement aperture located a few wavelengths apart from the array under test and being twice as large in size as the array length, the achievable resolution is generally larger than $\lambda/2$ [21], which in turn is the usual separation distance among the array elements. The limited resolution generally impairs the detection of isolated turned off elements that result masked by the reconstructions of adjacent functioning elements.

To improve the achievable resolution, the measurement aperture must be enlarged, or some methods borrowed from the array processing literature can be exploited [6], [22]. Among them, here we focus on the MUSIC algorithm because it fits the subtended localization problem well (due to the assumed turned on/turned off element fault type) and it is the key ingredient of the TR-MUSIC we aim to exploit.

As is well known, the MUSIC algorithm relies on the data correlation matrix $\mathbf{R} = \mathbf{e}\,\mathbf{e}^H$ whose eigenspectrum is used to single out the so-called noise subspace which in turn is exploited to build the MUSIC pseudospectrum indicator [5]. However, for the case at hand, $\mathbf{R}$ is clearly rank deficient with rank one. Consequently, if MUSIC is applied without a rank restoring procedure, a dramatic loss in the achievable performance is experienced. Indeed, MUSIC works no better than standard BTM or MM procedures (see [6] for theoretical arguments supporting this statement). To take advantage of the super-resolution ability of MUSIC, the rank of $\mathbf{R}$ must be recovered. This can be achieved by exploiting some de-correlation methods (i.e., smoothing procedures), which have been devised to deal with coherent or partially coherent signals [23]. Unfortunately, smoothing procedures cannot be directly exploited for near-field configurations. This limitation was overcome by the approach presented in [6], which basically casts the problem in the spatial Fourier domain and relies on the FFT of the measured data. However accurate FFT computation requires that the data be collected over a large aperture, preferably sampled uniformly over a dense $\lambda/2$ grid. Moreover, half the data are spent to achieve rank recovery.

In the sequel, we are concerned with a different, though MUSIC based diagnostic algorithm that can work without the need of the rank recovery step.

III. TIME-REVERSAL MUSIC DIAGNOSTIC ALGORITHM

Phased arrays are a kind of antenna that allows to steer the main beam. Usually, during the diagnostic stage, the array pattern is checked by changing the steering angle within the nominal field of view. From our perspective, this entails that further data are actually available and can be used in conjunction with or to reduce the spatial data. While the latter consideration applies whatever is the diagnostics algorithm, for the MUSIC this gives the further advantage that a rank recovery procedure is no longer necessary and hence all the related issues can be ignored.

To cast the previous discussion within a rigorous framework, assume that the field measurements are collected for L different steering angles. We call this data acquisition modality *steering diversity*. In particular, assume that the steering angles are chosen within the angular interval $AD = [-\theta_A, \theta_A]$. For example, for the l-th steering angle, θ_l, the field is expressed as

$$E_t(\mathbf{r}_{0m,\theta_l}) = \sum_{n=1}^{N-N_D} G_t(\mathbf{r}_{0m}, \mathbf{r}_{i_n}) e^{jkx_{i_n}\sin\theta_l} c_{i_n} \tag{5}$$

where N_D is the number of faulty elements and $S_D = (i_1, i_2, \cdots, i_{N-N_D}) \subseteq (1, 2, \cdots, N)$ is the subset of the properly functioning element indexes.

The overall field data result in L measurement vectors of size M that can be arranged in matrix form, $\mathbf{E}_t \in C^{M\times L}$, which in turn takes on the following factorized form

$$\mathbf{E}_t = \mathbf{GCS} \tag{6}$$

where $\mathbf{C} = diag\{\mathbf{c}\}$ is the diagonal $N - N_D \times N - N_D$ matrix obtained from the excitation coefficients $\mathbf{c}$, and $\mathbf{S} \in C^{N-N_D\times L}$ is the matrix whose columns collect the phase terms which steer the beam; more in detail, its $n - l$ entry is given by $S_{nl} = e^{jkx_{i_n}sin\theta_l}$.

It may be noted that $\mathbf{E}_t$, expressed in (6), resembles the so-called multi-static data matrix (MDM), which is the key ingredient of time-reversal imaging [16]. By virtue of this similarity, such a matrix in the sequel will be addressed again as MDM or more precisely as a multi-static multi-steering data matrix (MMDM). This similarity is by far more important since it allows to employ MUSIC to pursue the diagnostics without the need for a rank recovering procedure. This is because for $M, L \geq N - N_D$, $\mathbf{S}$ and $\mathbf{G}$ have rank $N - N_D$. For example, by uniformly sampling the steering term $u = \sin\theta$, $\mathbf{S}$ exhibits a Vandermonde structure, and thus its rank is $N - N_D$. For $\mathbf{G}$, because of the near-field configurations, the matter is quite tricky. Nonetheless, when the element factor is smooth (as is practically always the case) the structure of $\mathbf{G}$ is basically dictated by the scalar Green function terms (see (2)). In this case, there is abundant numerical and experimental evidence in literature that $\mathbf{G}$ is full rank [18]. Eventually, it can be concluded that the rank of $\mathbf{E}_t$ coincides with the number of non-defective elements. Let us regard the MMDM as a matrix operator, that is as

$$\mathbf{E}_t : \mathbf{a} \in C^{L\times 1} \rightarrow \mathbf{b} \in C^{M\times 1} \tag{7}$$

and assume that $L, M > N - N_D$. It clearly follows that

$$\begin{aligned} C^{M\times 1} &= R(\mathbf{E}_t) \oplus R(\mathbf{E}_t)^{\perp} \\ C^{L\times 1} &= R(\mathbf{E}_t^H) \oplus R(\mathbf{E}_t^H)^{\perp} \end{aligned} \tag{8}$$

where $R(\mathbf{E}_t)$ is the range of the matrix $\mathbf{E}_t$, $R(\mathbf{E}_t)^{\perp}$ its orthogonal complement and analogously for $\mathbf{E}_t^H$, with the superscript H denoting the Hermitian transpose. Often $R(\mathbf{E}_t)$ and $R(\mathbf{E}_t)^{\perp}$ are addressed in literature as the signal and the noise subspaces, respectively [6]. They can be separated through the singular value decomposition (SVD) of $\mathbf{E}_t$. In particular, in the noiseless case the signal subspace is spanned by the singular vectors corresponding to the singular values which are not zero.

Now, denote as $\mathbf{g}_n$ and as $\mathbf{a}_n$ $n = 1, 2, \ldots, N$, the column vectors of $\mathbf{G}$ and the row vectors of $\mathbf{S}$, respectively. According to the previous discussion, it results that $R(\mathbf{E}_t) = span\{\mathbf{g}_{i_1}, \cdots, \mathbf{g}_{i_n}, \cdots, \mathbf{g}_{i_{N-N_D}}\}$ and $R(\mathbf{E}_t^H) = span\{\mathbf{a}_{i_1}^H, \cdots, \mathbf{a}_{i_n}^H, \ldots.\mathbf{a}_{i_{N-N_D}}^H\}$. Moreover, denote as $\mathbf{u}_n$ and $\mathbf{v}_n$ the left and the right singular column vectors of $\mathbf{E}_t$ that span $R(\mathbf{E}_t)$ and $R(\mathbf{E}_t^H)$, respectively. Then, the properly

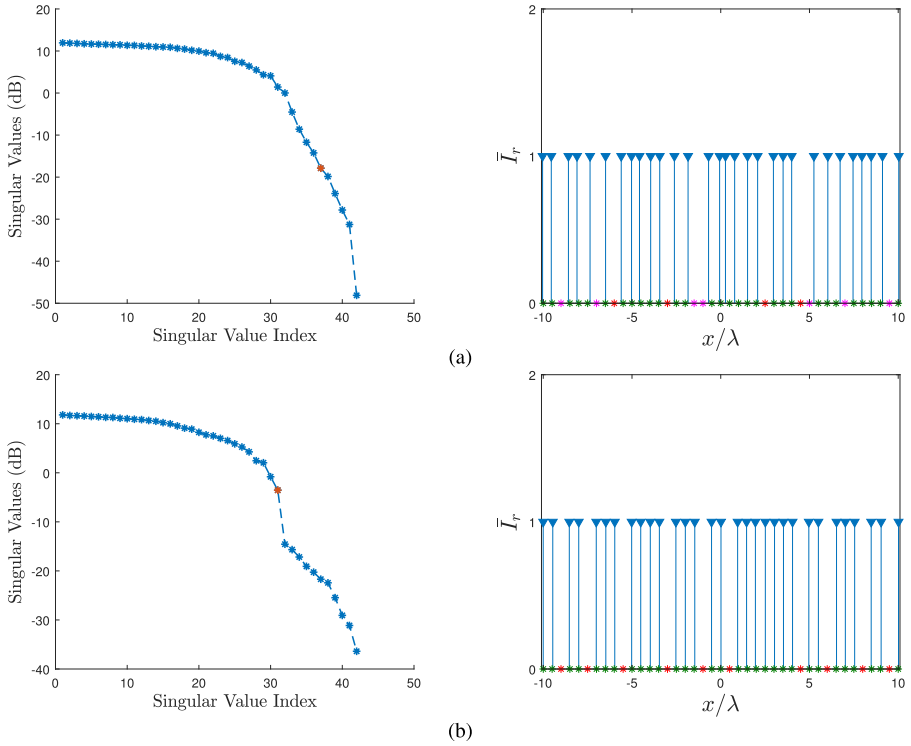

FIGURE 2. Left side of panel (a) and (b): singular values of matrix $\mathbf{E}_t$ associated to an array of $N = 41$ dipoles directed along the x axis and $\lambda/2$ spaced within a $SD = [-10\lambda, 10\lambda]$ for $N_D = 4$ and $N_D = 10$ faults respectively. The field is collected in $M = 65$ points uniformly spaced over $OD = [-16\lambda, 16\lambda]$ for $L = 65$ steering angle taken over $AD = [-\pi/2, \pi/2]$. Finally, a complex Gaussian noise with an $SNR = 30dB$ is added to the data. For this configuration it results $rank_{eff}(\mathbf{S}) = 41$ and $rank_{eff}(\mathbf{G}) = 37$. Right side panel (a) and (b): pseudospectrum associated to the considered array for $N_D = 4$ and $N_D = 10$ faults(red asterisks) respectively. The peaks of pseudospectrum, indicated by triangles, are associated with working elements(green asterisks). In panel (a) since $min(rank_{eff}(\mathbf{S}), rank_{eff}(\mathbf{G})) < N - N_D$, the algorithm failed to detect the working elements and appear false faults(magenta asterisks). Instead in panel (b) since $min(rank_{eff}(\mathbf{S}), rank_{eff}(\mathbf{G})) > N - N_D$ the algorithm allows to identify all the working elements.

functioning elements can be identified as the locus where the indicators (pseudospectra)

$$I_r(\mathbf{r}_n) = \frac{1}{1 - \sum_{\sigma_i \neq 0} |\mathbf{u}_i^H \tilde{\mathbf{g}}_n|^2} \tag{9}$$

and/or

$$I_\theta(\mathbf{r}_n) = \frac{1}{1 - \sum_{\sigma_i \neq 0} |\mathbf{v}_i^H \tilde{\mathbf{a}}_n^H|^2} \tag{10}$$

peak, with $\tilde{\mathbf{g}}_n = \mathbf{g}_n/||\mathbf{g}_n||$ and $\tilde{\mathbf{a}}_n = \mathbf{a}_n/||\mathbf{a}_n||$ being the normalized version of $\mathbf{g}_n$ and $\mathbf{a}_n$, representing the so-called steering vectors, σ_i are the singular values of $\mathbf{E}_t$. In particular, under the ideal noiseless case, exactly $N - N_D$ singular values are different from zero. In practice, the noise is always present and some threshold is to be employed to separate the signal and the noise singular values.

Accordingly, (9) and (10) are rewritten as

$$I_r(\mathbf{r}_n) = \frac{1}{1 - \sum_{\sigma_i > \epsilon} |\mathbf{u}_i^H \tilde{\mathbf{g}}_n|^2} \tag{11}$$

and

$$I_\theta(\mathbf{r}_n) = \frac{1}{1 - \sum_{\sigma_i > \epsilon} |\mathbf{v}_i^H \tilde{\mathbf{a}}_n^H|^2} \tag{12}$$

with ϵ being the separation threshold. Of course, the choice of the threshold impacts on the achievable performance.

A. EFFECTIVE RANK OF $\mathbf{E}_T$ AND THE ROLE OF NOISE

As discussed above, in the ideal noiseless case, the rank of $\mathbf{E}_t$ is equal to the number of properly functioning elements as long as both M, L are equal to or greater than that number. Therefore, if $M, L > N \geq N - N_D$, I_r and I_θ sharply peak at the working element positions.

When the noise enters the picture things can change drastically. In this case, the measurements are affected by the noise so that (4) actually is

$$\hat{\mathbf{E}}_t = \mathbf{E}_t + \mathbf{N} \tag{13}$$

where $\hat{\mathbf{E}}_t \in C^{M \times L}$ denotes the noisy MMDM matrix and $\mathbf{N} \in C^{M \times L}$ the noise matrix.

The noise clearly perturbs the singular spectrum of $\mathbf{E}_t$. The first obvious effect is that the zero singular values of

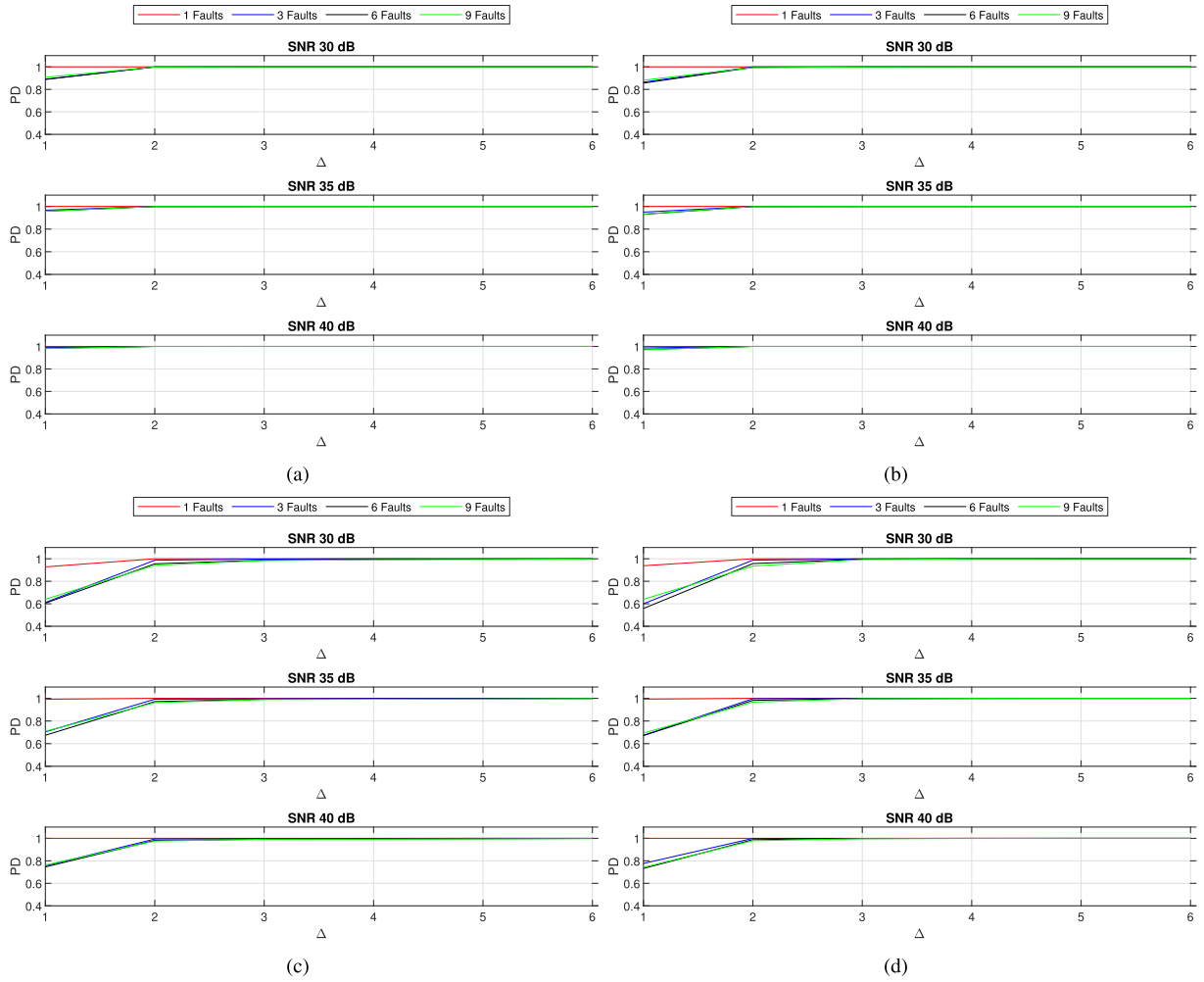

FIGURE 3. The probability of detection PD in terms of Δ returned by a Monte Carlo analysis performed over $N_{trials} = 1000$ trials. A linear phased array of $N = 41$ dipoles, uniformly spaced at $\lambda/2$ and arranged over the array support $SD = [-10\lambda, 10\lambda]$ is considered. The data are collected in $M = N_D + \Delta$ points uniformly spaced over $OD = [-16\lambda, 16\lambda]$. The steering angles are $L = rank_{eff}(\mathbf{S}) = 41$ selected by sampling the variable $sin\theta$ uniformly in the range $[-1, 1]$. There are only N_D amplitude failures and data are corrupted by noise. Both the noise and fault locations randomly change at each trial. In each sub-figure, the results for the SNR $\in \{30, 35, 40\}$ dB and $N_D \in \{1, 3, 6, 9\}$ are shown. Panels on the left refer to a uniform amplitude taper: in (a) the element factor is included in the estimation of I_r then in (c) it is neglected. Panels on the right refer to a Taylor amplitude taper with $SLL = 25dB$ and $\bar{n} = 4$: in (b) the element factor is included into the estimation of I_r, in (d) it is neglected.

$\mathbf{E}_t$ rise. This can make it difficult to distinguish between the noise and the signal subspaces. Accordingly, the ϵ threshold in (11) and (12) may not be easy to determine. Indeed, some literature methods can be employed to determine the singular values corresponding to the signal subspace but when the transition between the signal and the noise singular values is smooth their performance degrades [24]. A sufficient condition for the existence of a clear gap between the signal and the noise singular values can be derived by exploiting Weyl's theorem [25]. Denote as $\hat{\sigma}_i$s and σ_is the noisy and the noiseless singular values, then $|\hat{\sigma}_i - \sigma_i| \leq ||\mathbf{N}||_2$ $i = 1, 2, \cdots, min\{M, L\}$, which implies that $\hat{\sigma}_i \leq ||\mathbf{N}||_2$ for $i = N - N_D + 1, \cdots, min\{M, L\}$. Now, if $\sigma_{N-N_D} \gg 2||\mathbf{N}||_2$ then $\hat{\sigma}_{N-N_D} \gg \hat{\sigma}_{N-N_D+1}$ and there is a clear gap between the minimum signal singular value and the first noise one.

The role of noise can be even more serious. Indeed, even though the signal singular values were discernible or automatically selectable because the number of unknowns is a priori known, the noise perturbs the signal and the noise subspaces by the so-called out of space contribution [26]. Consequently, a significant performance degradation can occur. This drawback clearly depends on the available signal-to-noise ratio (SNR) but also on the characteristic of the noise. The most difficult scenario happens for single-snapshot measurement. For this case, an elegant formal treatment based on matrix perturbation theory [25] has been presented in [27] for the case of the MUSIC algorithm applied to a spectral estimation problem. There, for the case of well-resolved harmonics, meaning that they are separated more than Rayleigh's limits, the estimation error was provided in terms of the ratio between the minimum signal singular value

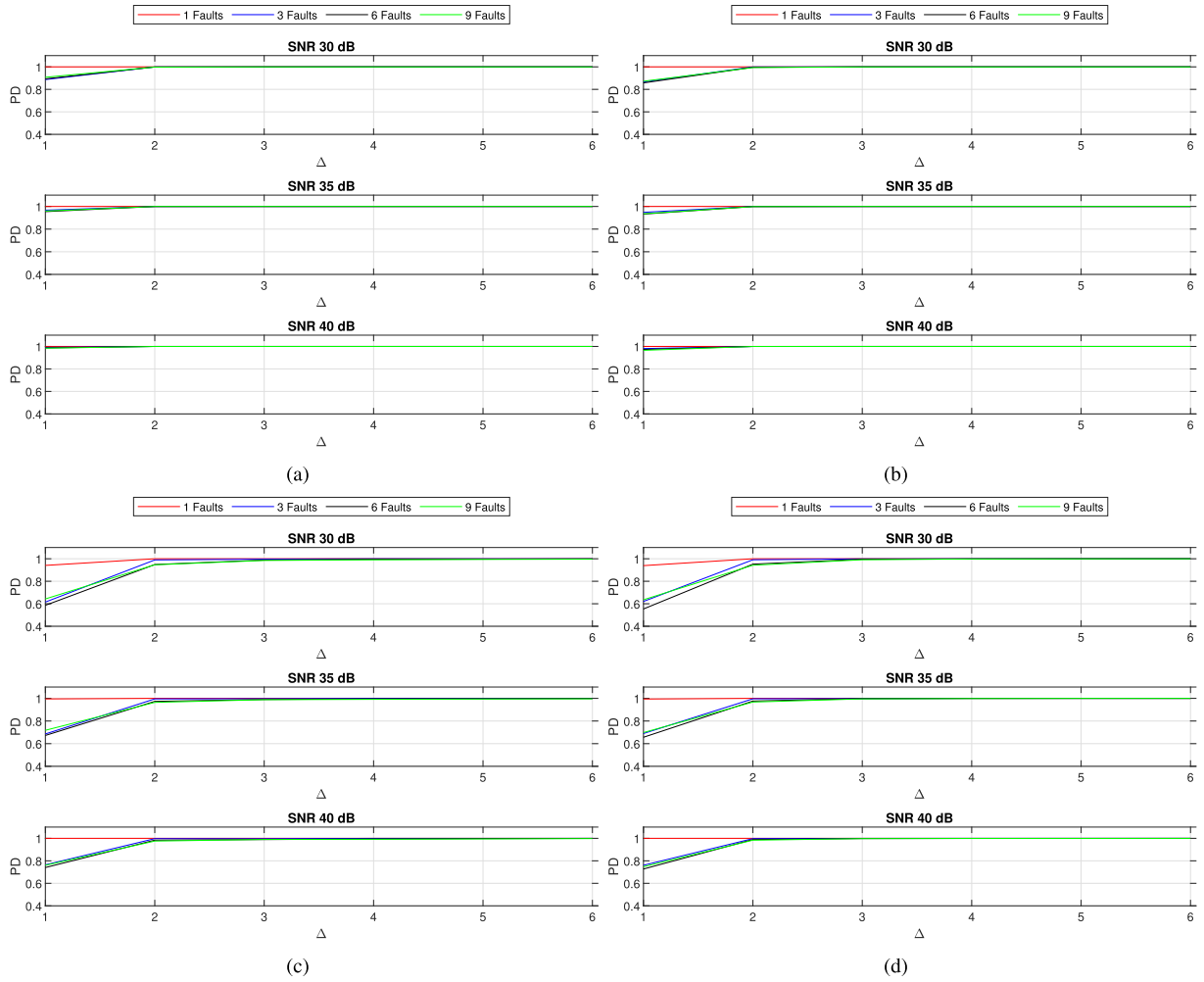

FIGURE 4. The probability of detection PD in terms of Δ returned by the same Monte Carlo analysis and measurements setup described in the caption of Fig.3. In this case, both amplitude and phase failures are considered. Panels on the left refer to a uniform amplitude taper: in (a) the element factor is included into the estimation of I_r then in (c) it is neglected. Panels on the right refer to a Taylor amplitude taper with $SLL = 25dB$ and $\bar{n} = 4$: in (b) the element factor is included into the estimation of I_r, in (d) it is neglected.

and the noise norm. Also, an estimation of the minimum singular value as a function of the number of the data samples and the harmonic amplitude dynamic range was provided.

In the multi-snapshots case, the problem simplifies since a simple averaging procedure allows to reduce the level of noise. Moreover, for uncorrelated zero mean noise samples (which is the case commonly assumed), the perturbation due to the noise while computing the singular value decomposition is close to a diagonal matrix so that the out of space perturbations become negligible. However, the measurement process is slowed down because measurements need to be collected multiple times for each position.

While the same estimation as in [27] cannot be directly exploited here, because the model is different and the array elements are in general not well-resolved, the very crucial role played by the minimum signal singular value, σ_{N-N_D}, also holds for the problem at hand. Eventually, if such a singular value is very low, then the TR-MUSIC performance may be insufficient even for a relatively high SNR. Unfortunately, this is just the case for the problem at hand due to the mathematical features of the radiation model.

Let us pause on this crucial point by elaborating more in depth on the rank of $\mathbf{G}$ and $\mathbf{S}$.

As discussed above, these matrices are full rank, that is $M, L > N - N_D \rightarrow rank(\mathbf{G}), rank(\mathbf{S}) = N - N_D$. However, depending on the configuration parameters, their *effective* rank can be lower than $N - N_D$, meaning that their singular values abruptly decay after a certain index.

More in detail, from the obvious link between $\mathbf{S}$ and the prolate spheroidal sequences [28], [29] it follows that its effective rank is

$$rank_{eff}(\mathbf{S}) \simeq \frac{2kX_s \sin(\theta_A)}{\pi} \tag{14}$$

As to $\mathbf{G}$, it is basically a discrete version of the radiation operator for which it has been shown that the singular values exhibit an almost step-like behavior [30]. Therefore, the effective rank can be estimated as the singular value index

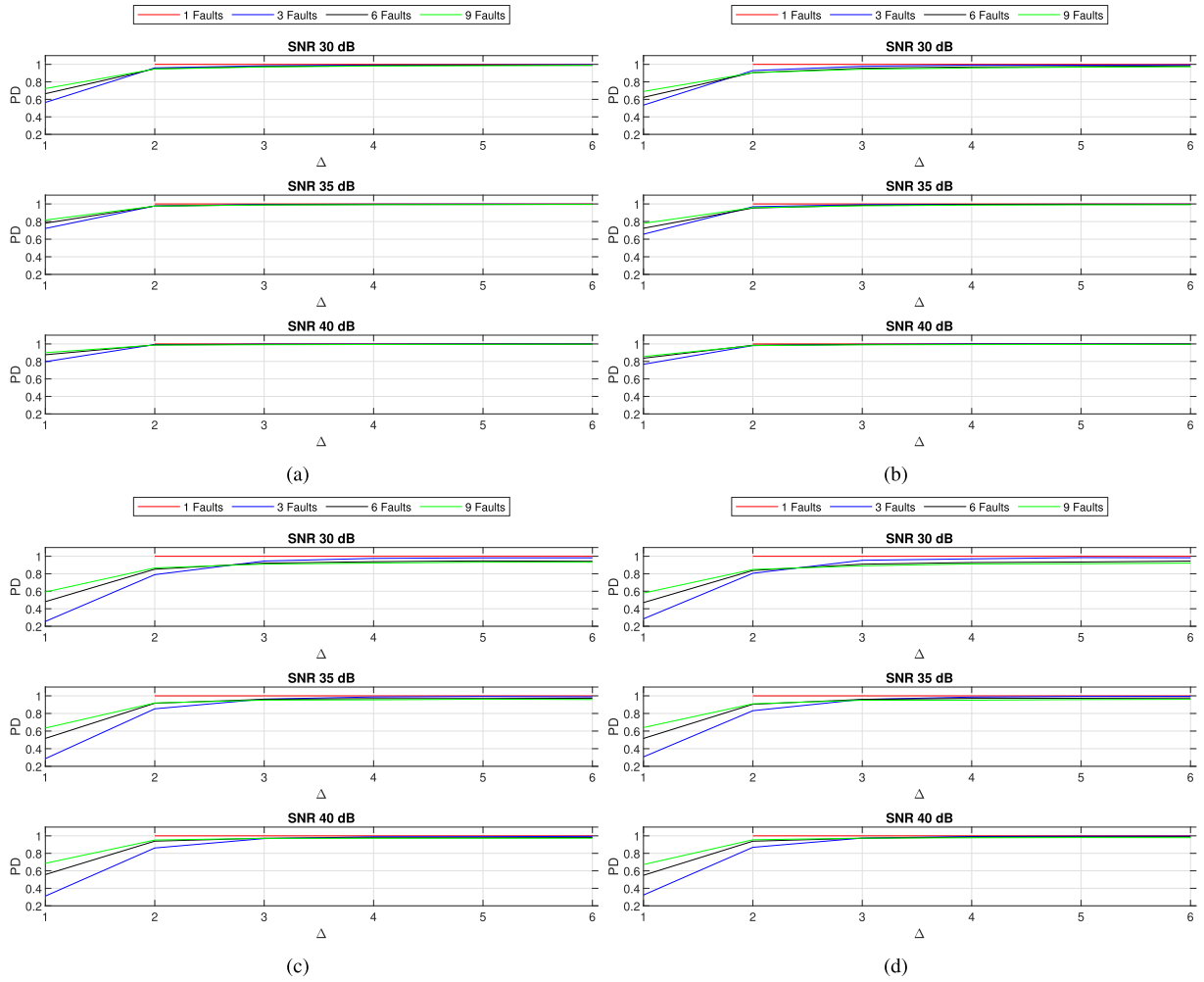

FIGURE 5. The probability of detection PD in terms of Δ returned by a Monte Carlo analysis performed over $N_{trials} = 1000$ trials. A linear phased array of $N = 41$ dipoles, uniformly spaced at $\lambda/2$ and arranged over the array support $SD = [-10\lambda, 10\lambda]$ is considered. The data are collected in $M = N_D + 2$ points uniformly spaced over $OD = [-16\lambda, 16\lambda]$. The steering angles are $L = N_D + \Delta$ selected over the Nyquist grid by enforcing the sampling to retain at least one pair at the Nyquist rate and the extreme points at -1 and 1. The other $L - 3$ angles are randomly chosen from the left samples of the Nyquist grid. Since at least 3 steering angle are needed, the curve associated to $N_D = 1$ start from $\Delta = 2$. Only N_D amplitude failures are considered. There is a noise in the data. Both the noise and fault locations randomly change at each trial. In each sub-figure, the results for the SNR $\in \{30, 35, 40\}$ dB and $N_D \in \{1, 3, 6, 9\}$ are shown. Panels on the left refer to an uniform amplitude taper: in (a) the element factor is included into the estimation of I_r, then in (c) it is neglected. Panels on the right refer to a Taylor amplitude taper with $SLL = 25dB$ and $\bar{n} = 4$: in (b) the element factor is included into the estimation of I_r, in (d) it is neglected.

where the *knee* occurs, that is as

$$rank_{eff}(\mathbf{G}) \simeq \frac{2}{\lambda}[\sqrt{(X_s + X_0)^2 + z_0^2} - \sqrt{(X_s - X_0)^2 + z_0^2}] \tag{15}$$

Now, by employing the Courant Fisher min-max theorem [31], it can be easily shown that

$$\sigma_{N-N_D}(\mathbf{E}_t) \leq min\{\sigma_{N-N_D}(\mathbf{G})|c_{max}|\sigma_1(\mathbf{S}), \sigma_1(\mathbf{G})|c_{max}|\sigma_{N-N_D}(\mathbf{S})\} \tag{16}$$

where we have used the notation $\sigma(\mathbf{A})$ to indicate that the singular values refer to the matrix $\mathbf{A}$ and $|c_{max}|$ is the maximum amplitudes of the excitation coefficients corresponding to the functioning elements. The upper bound in (16) is generally not tight and hence not useful to establish a sufficient condition for which the algorithm works. However, it allows to concluded that a necessary condition for the TR-MUSIC to work well is that

$$min(rank_{eff}(\mathbf{S}), rank_{eff}(\mathbf{G})) > N - N_D \tag{17}$$

If (17) does not hold true, because of (16), the minimum signal singular value, σ_{N-N_D}, is very low and thus even a low amount of noise can lead to a relevant performance degradation. The worst case happens when no faulty elements occur, that is for $N_D = 0$. In this case, the number of elements arranged over the aperture $[-X_s, X_s]$, for example according to the standard $\lambda/2$ distance, is $4X_s/\lambda$. Since, (15) tends to $4X_s/\lambda$ only when X_0 becomes unbounded, a very large measurement aperture would be required. Moreover, this

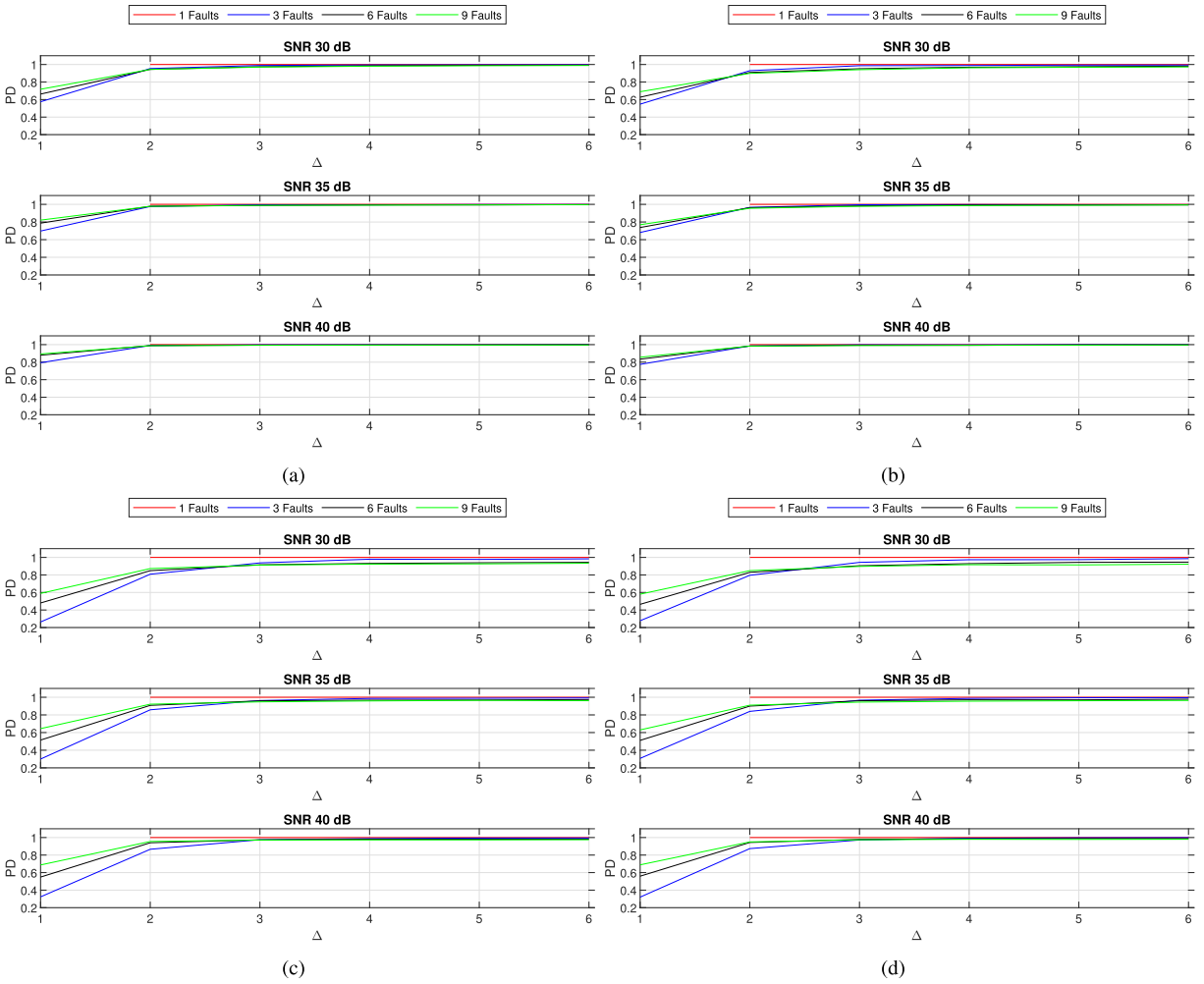

FIGURE 6. The probability of detection PD in terms of Δ returned by the same Monte Carlo analysis and measurements setup explained in the caption of Fig.5. In this case both amplitude and phase failures are considered. Panels on the left refer to an uniform amplitude taper: in (a) the element factor is included into the estimation of I_r, in (c) it is neglected. Panels on the right refer to a Taylor amplitude taper with $SLL = 25dB$ and $\bar{n} = 4$: in (b) the element factor is included into the estimation of I_r, in (d) it is neglected.

drawback cannot be in practice remedied by increasing the number of data, for example by exploiting a denser sampling grid, since increasing M and L much beyond N would only slowly increase the signal singular values [34]. To this end, the averaging procedure would be by far more effective and maybe more convenient to implement. Eventually, the present formulation of TR-MUSIC is expected to work as long as the number of defective elements is relatively (depending on the configuration parameters) high. Thus it can be considered as being complementary to other methods that address the case of few faults. It is worth pointing out that the mentioned limitation is not restricted to the TR-MUSIC but, being related to the mathematical features of the problem, affects any inversion method (i.e., BTM, MM, etc.), though in general with a different performance degradation.

We end this section by remarking that (14) and (15) can be verified with L and M only slightly larger than $rank_{eff}(\mathbf{S})$ and $rank_{eff}(\mathbf{G})$, respectively, if the $\mathbf{r}_{om}$ and the θ_l are properly selected. While it can easily be realized that the steering angle should be sampled so as to have a uniform step $\leq \pi/kX_s$ in $u = \sin\theta$, the determination of the spatial sampling positions is more involved because of the considered near-field configuration. Indeed, as it has been shown (for example in [32], [33]) the spatial samples should be collected according to a non-uniform rule.

B. OVERALL DETECTION ALGORITHM

In this section we briefly describe the steps the TR-MUSIC based detection algorithm consists of.

As mentioned above, the transition between the minimum signal singular value and the first noise singular value must be estimated in order to determine the noise subspace, which is in turn necessary for the formation of the pseudospectra (11) and (12). Therefore, the algorithm needs to be equipped with a procedure that achieves such a goal. In the noiseless case there is a very high gap between the mentioned singular values. In noisy cases, such a gap tends to be filled. However, it must still exist to have successful detection.

Therefore, to estimate the singular value transition index, we employ the difference vector $\Delta\sigma = [\sigma_1(\mathbf{E}_t) - \sigma_2(\mathbf{E}_t), \sigma_2(\mathbf{E}_t) - \sigma_3(\mathbf{E}_t), \cdots, \sigma_{N-1}(\mathbf{E}_t) - \sigma_N(\mathbf{E}_t)]$. Say i the index for which $\sigma_i(\mathbf{E}_t) - \sigma_{i+1}(\mathbf{E}_t)$ is maximum and set $\bar{i} = min\{i, rank_{eff}(\mathbf{G}), rank_{eff}(\mathbf{S})\}$. Then the noise subspace is estimated as the span of the singular vectors corresponding to singular values whose index ranges from $\bar{i}+1$ to $min\{M, L\}$.

The selected singular vectors are used to build the pseudospectra. In particular, this is achieved by considering a much finer grid (with respect to the array nominal grid). This allows to relax the need of a priori information about the array element positions as well as to deal with cases in which the elements positions are affected by uncertainties.

Finally, since TR-MUSIC allows for detection only, a standard peak picking procedure is employed and the results shown in binary form: 1 for detection and 0 for no-detection. The binary indicators are indicated as $\bar{I}_r$ and $\bar{I}_\theta$. The pseudocode algorithm is shown in Alg.1

C. ILLUSTRATIVE EXAMPLES

In order to support the previous theoretical discussion, in this section we show a couple of representative numerical examples.

An array of $N = 41$ dipoles directed along the x axis and uniformly spaced at $\lambda/2$ over the array support $[-X_s, X_s]$, $X_s = 10\lambda$, is considered. Uniform excitation distribution, that is $c_n = 1, \ \forall n$, is assumed, whereas the phase changes to implement the steering diversity. The steering angles are selected by uniformly sampling the variable $\sin\theta$ at $L = 42$ angles within the interval $[-1, 1]$. The radiated field is collected over $M = 42$ positions (for simplicity) uniformly deployed over a rectilinear observation domain with $X_0 = 16\lambda$ and located at $z_0 = 7\lambda$. Note that while L basically coincides with $rank_{eff}(\mathbf{S})$, M slightly exceeds $rank_{eff}(\mathbf{G})$. However, both M and L are greater than N; thus, in principle, the array with no fault can be addressed as well.

For noiseless data (not shown here), the TR-MUSIC always succeed in detecting and locating all the functioning elements, even when no faults are present. However, in practical cases, data are always corrupted by noise. Therefore, in the sequel data are perturbed by adding a zero mean complex white Gaussian noise matrix whose entries are independently generated according to the following rule

$$N_{nh} = \frac{\mathcal{N}(0,1) + j\mathcal{N}(0,1)}{\sqrt{2}} max\{|E_{tml}|\} 10^{-SNR/20} \qquad (18)$$

where $\mathcal{N}(0,1)$ denotes the normal distribution and $max\{|E_{tml}|\}$ is the noiseless data entry with the maximum amplitude.

Two cases with $N_D = 4$ and $N_D = 10$ faults (turned off elements) randomly introduced in the array are considered. The first case is chosen since the corresponding number of correctly functioning elements coincides with $min\{rank_{eff}(\mathbf{G}), rank_{eff}(\mathbf{S})\}$, whereas in the second case condition (17) is verified.

Algorithm 1 TR-MUSIC for Array Diagnostics From $\mathbf{E_t}$ Data

1: **function** Binary Pseudospectrum Indicator($\mathbf{E_t}$)
▷ $[\mathbf{u}, \sigma, \mathbf{v}]$ = SVD(*data*) is a function that return the singular system of *data*
▷ $[\mathbf{I}_r, \mathbf{I}_\theta]$ = PSD(*data*,SVD(*data*),signal subspace dimension) is a function that return the pseudospectra from the formula (11) and (12)
▷ [**pks**] = FINDPEAKS(*data*) is a function that return the peaks of vector *data*

2: $[\mathbf{u}, \sigma, \mathbf{v}] = \text{SVD}(\mathbf{E_t})$ ▷ Compute the SVD of the data
3: $\Delta\sigma = [\,]$ ▷ Initialize an empty vector

4: **for** j from 1 to length(σ) $-$ 1 **do**
5: $\Delta\sigma(j) = \sigma(j+1) - \sigma(j)$
6: **end for**

7: $i = max(abs(\Delta\sigma))$ ▷ Find the larger step in σ
8: $\bar{i} = min\{i, rank_{eff}(\mathbf{G}), rank_{eff}(\mathbf{S})\}$
9: ▷ Signal subspace dimension

10: $[I_r, I_\theta] = \text{PSD}(\mathbf{E}_t, \text{SVD}(\mathbf{E_t}), \bar{i})$
11: ▷ Build the pseudospectra
12:
13: **pks** $= [\,]$ ▷ Initialize an empty vector
14: [**pks**] = FINDPEAKS(I_r) ▷ Find peaks
15: pks = SORTDESCENDING(**pks**)
16: ▷ Sort in descending order **pks**

17: **for** k from 1 to $\bar{i}$ **do** ▷ Binary indicator
18: **for** each *index* of I_r **do**
19: **if** $I_r(index) == pks$(k) **then** $\bar{I}_r = 1$
20: **else**
21: $\bar{I}_r = 0$
22: **end if**
23: **end for**
24: **end for**

▷ Repeat from line 13 to 24 with I_θ instead of I_r

25: **return** $\bar{I}_r, \bar{I}_\theta$

26: **end function**

In both cases the SNR = 30 dB. It is worth remarking that this level of noise is considered reasonable for this type of problems [9]. Indeed, in lab conditions even a SNR as large as 60 dB is deemed feasible [10].

Finally, while constructing the pseudospectra the array aperture has been discretized by 3001 search points.

The outcome returned by the TR-MUSIC is reported in Fig. 2. The top row refers to the case of $N_D = 4$. As can be seen, the singular value behaviour does not show a clear

separation between the signal and the noise subspaces, though the selection procedure (i.e., algorithm step 2) returns the correct number of functioning elements (indicated by the singular value plotted by the red asterisks). Nonetheless, the indicator reported on the right panel shows inaccurate localization. Indeed, besides the actual faults (denoted by red asterisks), further faults (magenta asterisks) appear. Besides, some of the detected functioning elements show some deviation from their actual position. The bottom row of the same figure, instead, refers to the case of $N_D = 10$ faults. In this case, the noise subspace can be easily identified (see the left panel of row (b)) and the functioning elements are all detected and very precisely localized.

It is stressed that even by increasing the SNR till 60dB and/or the number of data the case of row (a) cannot be addressed successfully. This confirms that condition (17) must be strictly verified and that eventually the presented version of the TR-MUSIC is suited for the diagnostics of arrays populated by a relatively large number of faults.

IV. LOOKING FOR THE FAULTY ELEMENTS

As discussed above, the performance of the TR-MUSIC can be limited when dealing with a relatively small number of faulty elements. Since the latter is deemed to be more representative of practical scenarios, such a limitation needs to be overcome.

A common way to address the defective elements detection is by employing the difference model, which entails to look directly for the defective elements. The advantage is that the number of unknowns is dramatically reduced. However, the reference array, that is the array with all the elements properly functioning, must be known/estimated in someway. Also, a suitable processing scheme is necessary to gain advantage from the much lower number of data which are in principle required. In this framework, the inversion of the field data can be conveniently achieved by some CS algorithm [9].

Denote by $\mathbf{c}^r$ the excitation coefficients (with the steering term not included) of the reference array. Also, say $\mathbf{E}_t^r$ the corresponding MMDM. Then, the difference model is obtained as

$$\Delta\mathbf{E}_t = \mathbf{E_t} - \mathbf{E}_t^r = \mathbf{G}\Delta\mathbf{C}\mathbf{S} \tag{19}$$

with $\Delta\mathbf{C} = diag(\mathbf{c}_s)$, with $\mathbf{c}_s = \mathbf{c} - \mathbf{c}^r$. $\Delta\mathbf{E}_t$ can be seen as the field radiated by the *virtual* array whose active elements are only the defective elements.

In this case, we relax the assumption of turned off faulty elements. Hence, the defective elements can be of any type. In particular, the defective elements are represented as elements whose excitation coefficients are perturbed with respect to the reference ones, that is

$$c_n = c_n^r(1 + a_n)e^{j\phi_n} \tag{20}$$

with n ranging within the index set corresponding to the defective elements.

In this case, (17) rephrases as

$$min(rank_{eff}(\mathbf{S}), rank_{eff}(\mathbf{G})) > N_D \tag{21}$$

Since, $N_D \ll N$, (21) is easily verified. If (21) holds true the TR-MUSIC exhibits excellent detection and localization, with practically 100% probability of success when $SNR \geq$ 30 dB (not shown here for brevity). However, (21) implicitly entails that $M \geq rank_{eff}(\mathbf{G})$ and $L \geq rank_{eff}(\mathbf{S})$.

A. DATA REDUCTION

Condition (21) does not take into account the sparsity of the unknown $\mathbf{c}_s$, since $rank_{eff}(\mathbf{G})$ and $rank_{eff}(\mathbf{S})$ refer to the whole array grid. Though by a proper sampling strategy the number of data can be greatly reduced with respect to the $\lambda/2$ sampling [32], in view of the unknown sparsity, the amount of required data can be much lower. Indeed, the TR-MUSIC only needs $M, L > N_D$ to work.

The arising question is how to select such a reduced set of measurement positions. To this end, we select subsets of size M and L from the grids in $\mathbf{r}_{om}$ and u_l described at the end of section III-A. Since M, L can be much lower than N, if the measurement points and the angles are arranged to be contiguous, then the measurement aperture as well as the steering angular interval reduce. As a consequence, Rayleigh's limits expand and make the TR-MUSIC procedure more sensitive to the noise [27]. On the other hand, if the measurement aperture and the steering angular interval are kept the same, then a certain degree of under-sampling occurs. Accordingly, the pseudospectra can lead to false detection due to aliasing. This certainly holds true for I_θ. Instead, I_r is more resilient against this drawback. This is because the amplitude terms that appear in the spatial steering vectors, i.e., the $\mathbf{g}_n$s, help in distinguishing faults. Of course, when the noise enters the picture, the role of the amplitude terms can result smoothed. Therefore to achieve the detection of defective elements we considered

$$\bar{I}(\mathbf{r}_n) = \bar{I}_r(\mathbf{r}_n)\,\bar{I}_\theta(\mathbf{r}_n) \tag{22}$$

Using $I(\mathbf{r}_n)$ the false detection problem is strongly mitigated since aliasing in general affects $I_r(\mathbf{r}_n)$ and $I_\theta(\mathbf{r}_n)$ differently.

B. THE ROLE OF THE ELEMENT FACTOR

The element factor enters the data model. However, because of the array arrangement, the nominal element factor hardly coincides with the actual one. That is why, the active element factor is often employed. However, its estimation can be problematic so that usually simulations are employed. Also, the element factor depends on the actual array layout and hence can change according to the occurrence of the defective elements. This issue is not so serious for TR-MUSIC. Indeed, I_θ computation does not require the element factor. Instead, I_r weakly depends on it and can be obtained without knowing the element factor. This will be shown by numerical examples in the sequel.

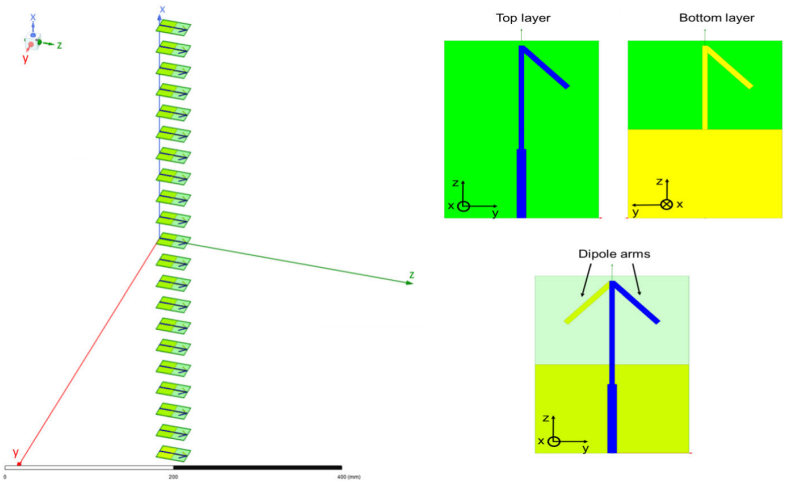

FIGURE 7. Left panel: Linear phased array array of $N = 21$ 45° angled printed dipole antenna, directed along the z axis and uniformly spaced at $\lambda/2$ over the array support $SD = [-5\lambda, 5\lambda]$. The working frequency is 5 GHz. Right panel: side views of the single dipole of the array. The images come from Ansys HFSS.

V. NUMERICAL ASSESSMENT: DATA REDUCTION AND THE ROLE OF THE ELEMENT FACTOR

In this section, we present the outcomes of an extensive set of numerical simulations devoted to assess the performance of the proposed diagnostic procedure against the data reduction and the lack of the element factor in I_r. All the examples deal with the array introduced in section III-C, consisting in $N = 41$ dipoles directed along the x axis and uniformly spaced at $\lambda/2$ over the support $[-X_s, X_s]$, with $X_s = 10\lambda$. The radiated field is collected over a rectilinear observation domain with $X_0 = 16\lambda$ and located at $z_0 = 7\lambda$. Again, the steering angles are selected by sampling the variable $\sin(\theta)$ within the interval $[-1, 1]$. Data are corrupted by an additive zero-mean white Gaussian noise, generated according to (18). In the examples, we consider two different tapers for the excitation coefficients: a uniform taper with $c_n = 1\ \forall n$ and a Taylor's taper with $SLL = 25dB$ and $\bar{n} = 4$. The considered faults can affect both the amplitude and phase of the excitation coefficients. They are taken into account by varying both a_n and ϕ_n in (20) according to the following probabilistic laws

$$a_n = -1 + 0.2\mathcal{N}(0, 1) \tag{23}$$

and

$$\phi_n = -\frac{\pi}{3} + \frac{2\pi}{3}\mathcal{N}(0, 1). \tag{24}$$

Evidently when only the amplitude is considered, ϕ_n is set to zero $\forall n$.

The outcomes have been evaluated by running the diagnostic procedures for different values of $N_D = \{1, 3, 6, 9\}$ and $SNR \in \{30, 35, 40\}dB$. For each value of N_D and SNR, a Monte Carlo analysis is performed by repeating the diagnostics $N_{Trials} = 1000$ times and by randomly changing the fault locations and the noise realization. The performances of the approach have been quantitatively evaluated by the probability of detection (PD)

$$\text{PD} = \frac{1}{N_{Trials}} \sum_{n=1}^{N_{Trials}} \frac{\text{FD}(n)}{N_D} \tag{25}$$

where FD denotes the number of detected faults. Two different data sampling strategies are considered. In case A, data are collected over $M = N_D + \Delta$ positions uniformly deployed over OD and with Δ the surplus of data against N_D, instead steering angles are selected at $L = rank_{eff}(\mathbf{S})$ angles. In case B, both M and L are reduced and controlled by the number of faults. Both results achieved with and without the element factor in I_r are shown.

A. PD EVALUATION: CASE A

In these numerical examples, the steering angles are selected at $L = rank_{eff}(\mathbf{S}) = 41$ angles that represents the Nyquist number. On the contrary, near field data are collected over $M = N_D + \Delta$ positions. Note that M is mainly controlled by the number of faults and it can be lower than $rank_{eff}(\mathbf{G}) = 37$ resulting into an under-sampling of data. First of all, we focus on detecting only amplitude faults. We start by considering an array with a uniform taper. The achieved probabilities of detection (PDs) in terms of Δ are shown in panel (a) and (c) of Fig. 3. In particular, the results in panel (a) are achieved by including the element factor in I_r, in panel (c) without it. As can be seen, in the case of a single fault, only $M = 2$ measurements are required to achieve a high PD. As N_D increases, a $\Delta \geq 2$ ensures a PD close to 1, by adding more measurements, PD reaches 1. Note that only when $\Delta = 1$, the lack of the element factor compensation affects the results, as $\Delta \geq 2$, the performances are close to the other case. It must be pointed out that in order to achieve these large values of PD, we need $M = \{2, 5, 8, 11\}$ (depending

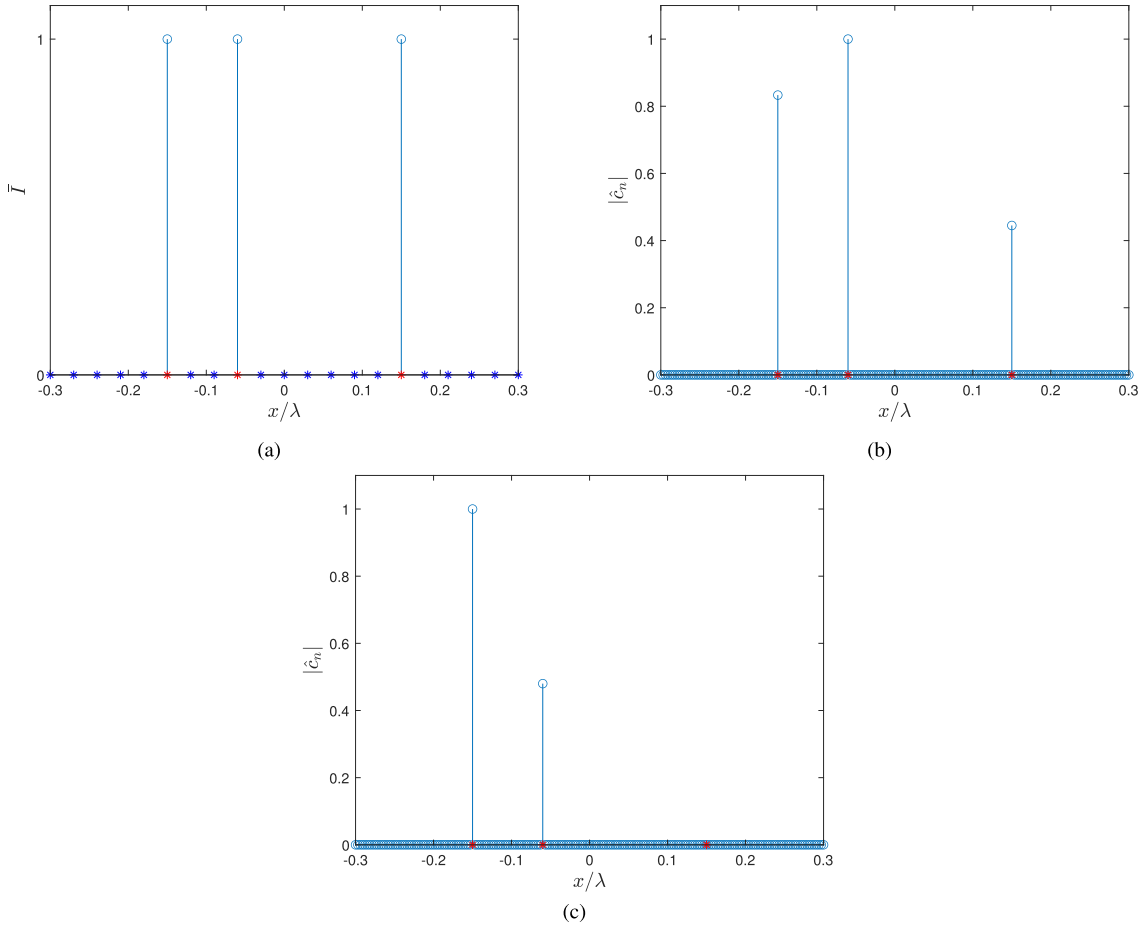

FIGURE 8. Comparison between TR-MUSIC algorithm and CS methods. $N_D = 3$ faulty elements (red asterisks) are considered in the array shown in Fig.7. The other parameters are $OD = [-8\lambda, 8\lambda]$ and $z_0 = 7\lambda$. The number of data is ML with $M = 5$ and $L = 6$ collected with the sampling strategy described in Fig.5. The data are noisy with $SNR = 35dB$. Panel(a): Binary pseudospectrum indicator $\bar{I}$ using TR-MUSIC. Panel (b) and (c): Reconstructed coefficient using CS with regularization parameter $\epsilon_r = 4.55$ and $\epsilon_r = 5.54$ respectively. Notice that in panel c) we are not able to detect all the faults due to a wrong choice of regularization parameter instead of panel b) the detection is clear.

on N_D), numbers highly lower than $rank_{eff}(\mathbf{G})$. Accordingly, we succeed in fault detection with a reduced number of near field measurements. Moreover, the performance is quite the same regardless of the *SNR* and the lack of element factor compensation. The stability of the approach against the noise is expected thanks to the considered sampling strategy that keeps the measurement aperture unchanged.

Now let's consider Taylor's current taper. For this type of taper, it is difficult to distinguish the faults from excitation coefficients, especially where the latter are very low. Accordingly, standard approaches often fail to detect them.

However, this degradation is not observed in TR-MUSIC. In fact, as can be seen in panels (b) and (d) of Fig.3 results similar to the amplitude taper can be achieved.

Now, we consider both amplitude and phase faults. Again the PD in terms of Δ are shown in Fig.4. In the panels on the left, the results concerning the uniform taper obtained with and without the element factor (top and bottom panel, respectively) are shown, and on the right the Taylor one. As can be seen, similar results as before can be obtained. A Δ larger than 2 is sufficient to reach a very large probability of detection.

This set of simulations confirms the capability of TR-MUSIC of detecting any type of defect by a reduced number of near field measurements. Moreover, the lack of the element factor is not such a serious issue for it. As pointed out in the introduction, since beam scanning is achieved at *electronic speed*, the data acquisition time is mainly dominated by the one necessary to collect spatial data. Accordingly, their reduction can significantly speed up the diagnostic procedure. However, according to theoretical results, the TR-MUSIC only needs $M, L > N_D$ to work. This means that also the number of steering angles can be reduced.

B. PD EVALUATION: CASE B

In order to assess the performance of the proposed approach against the reduction of steering angle number, we suppose to set $M = N_D + 2$ and $L = N_D + \Delta$. Accordingly, L can be lower than $rank_{eff}(\mathbf{S}) = 41$, so an under-sampling can

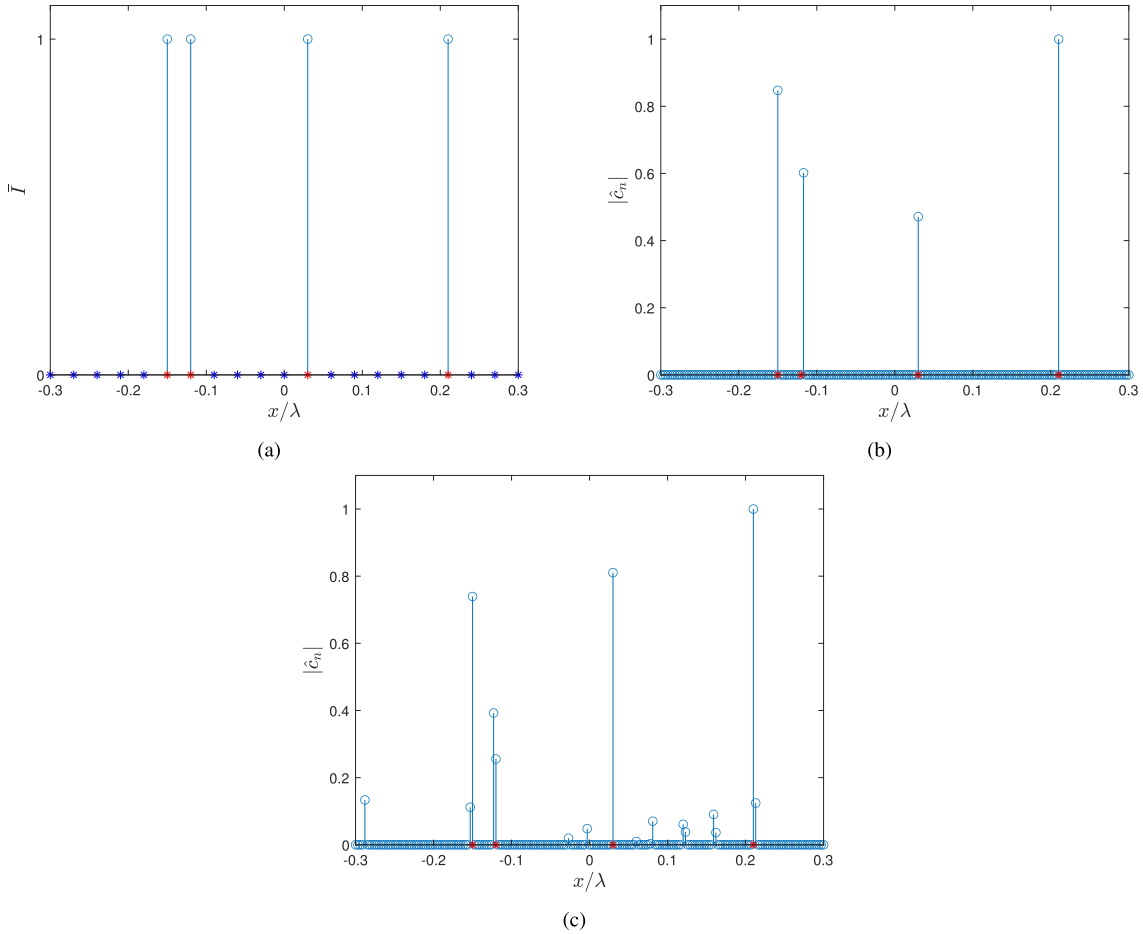

FIGURE 9. Comparison between TR-MUSIC algorithm and CS methods. $N_D = 4$ faulty elements (red asteriks) are considered in the array shown in Fig.7. The measurements parameter are the same as in Fig.8 Panel(a): Binary pseudospectrum indicator $\bar{I}$ using TR-MUSIC. Panel (b) and (c): Reconstructed coefficient using CS with regularization parameter $\epsilon_r = 5.54$ and $\epsilon_r = 4.55$ respectively. Again a wrong choice of regularization parameter fails in the detection as reported in panel c).

occur. As detailed in section IV, compared to the previous case, the under-sampling in I_θ is more critical. In fact, if the steering angles are selected by sampling uniformly $\sin\theta$ in $[-1, 1]$, the under-sampling gives rise to the same phase in $\tilde{\mathbf{a}}_n = \mathbf{a}_n/||\mathbf{a}_n||$ for different fault testing positions, resulting in false detection in I_θ. To address this issue, the steering angles are randomly selected over the Nyquist grid (uniform step equal to $\pi/(kX_s)$) by enforcing the sampling to retain at least one pair at the Nyquist rate and the extreme points at -1 and 1. This means that at least 3 steering angles are necessary. With that in mind, we perform the same numerical analysis as before, by focusing first on the scenario with only amplitude failures for uniform taper and the Taylor's one. The results with and without the element factor compensation are shown in Fig.5. By comparing the latter to Fig.3, a slight reduction in probability of detection is observed especially for $SNR = 30dB$ and without the element factor compensation. It's essential to highlight that, compared to scenarios where all steerings were considered, the amount of available data significantly decreases, specifically to $(N_D + 2)(N_D + \Delta)$. Accordingly, a slight degradation in performance is expected. However, a $\Delta \geq 3$ is sufficient to guarantee a PD close to 1. In Fig. 6, P_D is shown for both amplitude and phase faults. The results are aligned to the trends observed before. This confirms the algorithm's effectiveness, even when a reduced number of steering angles is considered.

According to the previous discussion, the total number of data ML guaranteeing a P_D close to 1 is equal to $(N_D + 2)(N_D + 3)$. This probability also occurs when the element factor is not included in the evaluation of I_r.

VI. TR-MUSIC VS COMPRESSIVE SENSING

Since the difference model promotes the sparsity of the unknown, the proposed approach is compared to CS algorithm. In particular, the latter is applied to (19) by stacking the data coming from different steering angles to create a single data vector. So the faulty element coefficients are determined by considering the following model

$$vec(\Delta\mathbf{E}_t) = \mathbf{S}^t * \mathbf{G}\Delta\mathbf{c}_s \tag{26}$$

where $vec(\cdot)$ denote the vectorization of the matrix argument, $*$ is the column-wise Khatri–Rao product and $(\cdot)^t$ means

the transpose matrix. Let us consider an array composed of $N = 21$ 45° angled printed dipole antenna, directed along the z axis and uniformly spaced at $\lambda/2$ over the support $X_s = 5\lambda$ and working at 5 GHz as sketched in Fig. 7. The observation domain is parallel to the array, located at $z_0 = 7\lambda$ and with size $X_0 = 8\lambda$. The field radiated by this array has been computed with the full wave 3D electromagnetic software Ansys HFSS [35] for $M = (N_D+2)$ points over OD and $L = N_D + 3$ different steering angles sampled according to the strategy discussed in the previous sections. Finally the ML data are corrupted by an additive zero mean white Gaussian noise, generated according to (18) with $SNR = 35dB$. Note that for this type of radiating element, the nominal factor is not known in closed form. Accordingly, it should be numerically estimated. In order to avoid this step, we suppose to neglect it in both the diagnostic approaches. So for CS algorithm we solve the following minimization problem using

$$\min_{\Delta \mathbf{c}_s} ||\Delta \mathbf{c}_s||_1 \quad \text{subject to} \quad ||\mathbf{A}\Delta \mathbf{c}_s - vec(\Delta \mathbf{E}_t)||_2 \leq \epsilon_r \quad (27)$$

where $\mathbf{A} = \mathbf{S}^t * \bar{\mathbf{G}}$, $\bar{\mathbf{G}}$ is the matrix $\mathbf{G}$ without the element factor, ϵ_r is the regularization parameter and $||\cdot||_1$ indicate the l_1 norm. To solve problem (27) we used CVX, a package for specifying and solving convex programs [36], [37]. Of course, we pass from a coefficient estimation to a mere detection due to the lack of element factor that enters in the definition of the entries of $\mathbf{G}$. This is indeed true for any other reconstruction procedure. In order to simulate faulty elements, a number of $N_D = 3$ and $N_D = 4$ elements are completely turned off. The detection results are shown in Fig.8 and Fig.9. In particular, panel a) refers to TR-MUSIC, panel b) and c) to CS algorithm for different value of ϵ_r. Both the approaches allow to achieve the fault detection. However, the CS algorithm needs the setting of the regularization parameter. Typically, since the latter represents the data fitting constraint, it should be set larger than the norm of the noise but, in this case, the data fitting error should contemplate also the lack of element factor. Accordingly, it is very difficult to set it. Moreover, its best value can be affected by both the number and layout of faults that are unknowns of the problem, making the CS algorithm unpractical to be exploited in realistic scenario. In fact for the layout in Fig.8 the best regularization parameter is $\epsilon_r = 4.55$, then in Fig.9 is $\epsilon_r = 5.54$. On contrary, the proposed approach does not require any optimization procedure and no regularization term must be set. Another advantage of TR-MUSIC is its low computational effort. In fact, while CS algorithm needs to built the matrix $\mathbf{A}$ whose size is $ML \times N$, in the proposed approach, the data matrix is only $M \times L$ in size. Finally, the TR-MUSIC, as well as other similar approaches, is often addressed in literature as a *grid-less* method. Basically, this refers to the fact that the grid of points over which the unknown is supported only enters during the pseudospectrum formation and needs not to be stored since the beginning. Note that this is not the case for CS algorithm or other approaches based on a direct inversion of (26), which instead requires the matrix model to be stored in advance.

VII. CONCLUSION

In this paper, a novel strategy for the detection of faulty elements in a phased array from near-field measurements has been proposed. In this type of array, it is possible to introduce the steering diversity. Accordingly, by collecting the radiated field over the measurement aperture while steering the beam, the TR-MUSIC algorithm is borrowed by the signal processing and exploited to achieve the diagnostics. In particular, it can be applied to look for the working elements or the defective ones. In the first case, the TR-MUSIC is expected to work for the detection of completely turned off elements as long as the number of defective elements is relatively (depending on the configuration parameters) high. Thus it can be considered as being complementary to other methods that address the case of few faults.

Instead when the case of few faults is considered, TR-MUSIC can be applied to the difference model. In this case, it succeeds in detecting any type of failure by a reduced set of data, mainly depending on the number of faulty elements. Performance in terms of detection probability was analysed by means of Monte Carlo numerical analysis. In particular, through this analysis, we concluded that the total number of spatial data that guarantees a probability of detection close to 1 is equal to $(N_D + 2)$(with at least $(N_D + 3)$ steering angles). This probability also occurs when the element factor is not included in the evaluation of I_r. In fact, because of the array arrangement, in the practical case, the nominal element factor hardly coincides with the actual one, so it must be estimated. Its estimation can be problematic because the element factor depends on the actual array layout and hence can change according to the occurrence of the defective elements. It is shown that this issue is not so serious for TR-MUSIC that always works. On contrary, for CS algorithm, the lack of the element factor in the model affects the choice of the regularization parameter. Accordingly, it is very difficult to set it and its best value can be affected by both the number and faults layout that are unknowns of the problem, making the CS algorithm unpractical to be exploited in a realistic scenario. Another advantage of TR-MUSIC is its low computational effort, in fact, it works with a matrix lower in size than CS. Finally, for the TR-MUSIC, the grid of points over which the unknown is supported only enters during the pseudospectrum formation and need not be stored since the beginning. Note that this is not the case for CS algorithm or other similar approaches, which instead require the matrix model to be stored in advance.

REFERENCES

[1] J. R. Mohammed and A. J. Abdulqader, "Array pattern restoration under defective elements," *Prog. Electromagn. Res. C*, vol. 123, pp. 17–26, 2022, doi: 10.2528/pierc22061101.

[2] J. R. Mohammed, "A method for thinning useless elements in the planar antenna arrays," *Prog. Electromagn. Res. Lett.*, vol. 97, pp. 105–113, 2021, doi: 10.2528/pierl21022104.

[3] J. J. Lee, E. M. Ferren, D. P. Woollen, and K. M. Lee, "Near-field probe used as a diagnostic tool to locate defective elements in an array antenna," *IEEE Trans. Antennas Propag.*, vols. AP-36, no. 6, pp. 884–889, Jun. 1988, doi: 10.1109/8.1192.

[4] O. M. Bucci, M. D. Migliore, G. Panariello, and P. Sgambato, "Accurate diagnosis of conformal arrays from near-field data using the matrix method," *IEEE Trans. Antennas Propag.*, vol. 53, no. 3, pp. 1114–1120, Mar. 2005, doi: 10.1109/tap.2004.842656.

[5] A. Buonanno and M. D'Urso, "A novel strategy for the diagnosis of arbitrary geometries large arrays," *IEEE Trans. Antennas Propag.*, vol. 60, no. 2, pp. 880–885, Feb. 2012, doi: 10.1109/TAP.2011.2173109.

[6] A. Dell'Aversano, A. Natale, A. Cuccaro, and R. Solimene, "Linear array antenna diagnostics through a MUSIC algorithm," *IEEE Access*, vol. 7, pp. 176952–176959, 2019, doi: 10.1109/ACCESS.2019.2956680.

[7] R. Solimene, M. A. Maisto, and R. Pierri, "Sampling approach for singular system computation of a radiation operator," *J. Opt. Soc. Amer. A, Opt. Image Sci.*, vol. 36, no. 3, p. 353, Mar. 2019, doi: 10.1364/josaa.36.000353.

[8] M. Maisto, R. Pierri, and R. Solimene, "Near-field warping sampling scheme for broad-side antenna characterization," *Electronics*, vol. 9, no. 6, p. 1047, Jun. 2020, doi: 10.3390/electronics9061047.

[9] M. D. Migliore, "A compressed sensing approach for array diagnosis from a small set of near-field measurements," *IEEE Trans. Antennas Propag.*, vol. 59, no. 6, pp. 2127–2133, Jun. 2011, doi: 10.1109/TAP.2011.2144556.

[10] B. Fuchs, L. L. Coq, and M. D. Migliore, "Fast antenna array diagnosis from a small number of far-field measurements," *IEEE Trans. Antennas Propag.*, vol. 64, no. 6, pp. 2227–2235, Jun. 2016, doi: 10.1109/TAP.2016.2547023.

[11] M. Salucci, A. Gelmini, G. Oliveri, and A. Massa, "Planar array diagnosis by means of an advanced Bayesian compressive processing," *IEEE Trans. Antennas Propag.*, vol. 66, no. 11, pp. 5892–5906, Nov. 2018, doi: 10.1109/TAP.2018.2866534.

[12] W. Li, W. Deng, Q. Yang, and M. D. Migliore, "Fast non-convex compressed sensing approach for diagnosis of defective array elements using planar near-field measurements," *IET Microw., Antennas Propag.*, vol. 13, no. 11, pp. 1940–1947, Sep. 2019, doi: 10.1049/iet-map.2019.0008.

[13] V. Schenone, A. Fedeli, C. Estatico, M. Pastorino, and A. Randazzo, "Detection of failures in antenna arrays through a lebesgue-space approach," *IEEE Open J. Antennas Propag.*, vol. 3, pp. 652–662, 2022. [Online]. Available: https://ieeexplore.ieee.org/document/9790805, doi: 10.1109/OJAP.2022.3181345.

[14] R. Palmeri, G. M. Battaglia, A. F. Morabito, S. Costanzo, F. Venneri, and T. Isernia, "Fault diagnosis of realistic arrays from a reduced number of phaseless near-field measurements," *IEEE Trans. Antennas Propag.*, vol. 70, no. 9, Sep. 2023, Art. no. 72067219, doi: 10.1109/TAP.2023.3293004.

[15] C. Xiong, G. Xiao, Y. Hou, and M. Hameed, "A compressed sensing-based element failure diagnosis method for phased array antenna during beam steering," *IEEE Antennas Wireless Propag. Lett.*, vol. 18, pp. 1756–1760, 2019, doi: 10.1109/LAWP.2019.2929353.

[16] A. J. Devaney, "Time reversal imaging of obscured targets from multistatic data," *IEEE Trans. Antennas Propag.*, vol. 53, no. 5, pp. 1600–1610, May 2005, doi: 10.1109/tap.2005.846723.

[17] F. K. Gruber, E. A. Marengo, and A. J. Devaney, "Time-reversal imaging with multiple signal classification considering multiple scattering between the targets," *J. Acoust. Soc. Amer.*, vol. 115, no. 6, pp. 3042–3047, Jun. 2004, doi: 10.1121/1.1738451.

[18] M. A. Maisto, R. Solimene, and R. Pierri, "Resolution limits in inverse source problem for strip currents not in Fresnel zone," *J. Opt. Soc. Amer. A, Opt. Image Sci.*, vol. 36, no. 5, p. 826, May 2019, doi: 10.1364/josaa.36.000826.

[19] M. D. Prete and G. Leone, "Planar phased array antenna diagnostics by a MUSIC-based algorithm," in *Proc. IEEE Conf. Antenna Meas. Appl. (CAMA)*, Dec. 2022, pp. 1–3, doi: 10.1109/CAMA56352.2022.10002621.

[20] M. Del Prete, M. A. Maisto, and G. Leone, "Data reduction in linear phased array diagnostic by a TR-MUSIC based approach," in *Proc. 17th Eur. Conf. Antennas Propag. (EuCAP)*, Mar. 2023, pp. 1–4, doi: 10.23919/EuCAP57121.2023.10133334.

[21] M. A. Maisto, R. Pierri, and R. Solimene, "Near-field transverse resolution in planar source reconstructions," *IEEE Trans. Antennas Propag.*, vol. 69, no. 8, pp. 4836–4845, Aug. 2021, doi: 10.1109/TAP.2021.3060030.

[22] R. Roy and T. Kailath, "ESPRIT-estimation of signal parameters via rotational invariance techniques," *IEEE Trans. Acoust., Speech, Signal Process.*, vol. 37, no. 7, pp. 984–995, Jul. 1989, doi: 10.1109/29.32276.

[23] S. U. Pillai and B. H. Kwon, "Forward/backward spatial smoothing techniques for coherent signal identification," *IEEE Trans. Acoust., Speech, Signal Process.*, vol. 37, no. 1, pp. 8–15, Jan. 1989, doi: 10.1109/29.17496.

[24] M. Davy, J.-G. Minonzio, J. de Rosny, C. Prada, and M. Fink, "Influence of noise on subwavelength imaging of two close scatterers using time reversal method: Theory and experiments," *Prog. Electromagn. Res.*, vol. 98, pp. 333–358, 2009, doi: 10.2528/pier09071004.

[25] V. N. Bogaevski and A. Povzner, "Matrix perturbation theory," in *Applied Mathematical Sciences*. New York, NY, USA: Academic, 1991, pp. 1–15.

[26] D. Ciuonzo, G. Romano, and R. Solimene, "Performance analysis of time-reversal MUSIC," *IEEE Trans. Signal Process.*, vol. 63, no. 10, pp. 2650–2662, May 2015, doi: 10.1109/TSP.2015.2417507.

[27] W. Liao and A. Fannjiang, "MUSIC for single-snapshot spectral estimation: Stability and super-resolution," *Appl. Comput. Harmon. Anal.*, vol. 40, no. 1, pp. 33–67, Jan. 2016, doi: 10.1016/j.acha.2014.12.003.

[28] H. J. Landau and H. O. Pollak, "Prolate spheroidal wave functions, Fourier analysis and uncertainty—III: The dimension of the space of essentially time-and band-limited signals," *Bell Syst. Tech. J.*, vol. 41, Oct. 1962, Art. no. 12951336.

[29] D. Slepian, "Prolate spheroidal wave functions, Fourier analysis and uncertainty—IV: Extensions to many dimensions; generalized prolate spheroidal functions," *Bell Syst. Tech. J.*, vol. 43, no. 6, pp. 3009–3057, Nov. 1964, doi: 10.1002/j.1538-7305.1964.tb01037.x.

[30] R. Solimene, M. A. Maisto, and R. Pierri, "Inverse source in the near field: The case of a strip current," *J. Opt. Soc. Amer. A, Opt. Image Sci.*, vol. 35, no. 5, p. 755, May 2018, doi: 10.1364/josaa.35.000755.

[31] E. H. Lieb and M. Loss, *Analysis (Graduate Studies in Mathematics)*, 2nd ed. Providence, RI, USA: American Mathematical Society, 2001.

[32] M. A. Maisto, G. Leone, A. Brancaccio, and R. Solimene, "Efficient planar near-field measurements for radiation pattern evaluation by a warping strategy," *IEEE Access*, vol. 9, pp. 62255–62265, 2021, doi: 10.1109/ACCESS.2021.3074786.

[33] M. A. Maisto, M. Del Prete, G. Leone, R. Pierri, and R. Solimene, "Non-uniform warping sampling for data reduction in planar array diagnostics," *IEEE Access*, vol. 10, pp. 82336–82345, 2022, doi: 10.1109/ACCESS.2022.3196384.

[34] R. C. Thompson, "The behavior of eigenvalues and singular values under perturbations of restricted rank," *Linear Algebra Appl.*, vol. 13, nos. 1–2, pp. 69–78, 1976.

[35] *Ansys Electromagnetics Suite*, ANSYS Inc., Canonsburg, PA, USA, 2021.

[36] M. Grant and S. Boyd. (2013). *CVX: MATLAB Software for Disciplined Convex Programming*. [Online]. Available: http://cvxr.com/cvx

[37] M. C. Grant and S. P. Boyd, "Graph implementations for nonsmooth convex programs," in *Lecture Notes in Control and Information Sciences*. Cham, Switzerland: Springer, 2008, pp. 95–110.

MARIA ANTONIA MAISTO (Member, IEEE) received the M.S. degree (summa cum laude) in electronic engineering and the Ph.D. degree in electronic and computer science engineering from the University of Campania, Aversa, Italy, in 2012 and 2015, respectively. Since 2016, she has been holding a Postdoctoral Fellowship with the Department of Engineering, Universitã della Campania. Her current research interest includes electromagnetic inverse problems, with a particular attention to theoretical and numerical aspects. In particular, she include electromagnetic inverse source and inverse scattering problems, electromagnetic field information content, microwave radar imaging, RCS estimation from near-field measurements, and electromagnetic field sampling.

MARIO DEL PRETE (Student Member, IEEE) received the M.S. degree (summa cum laude) in electronic engineering from the University of Campania, Aversa, Italy, in 2021. He is currently pursuing the Ph.D. degree in industrial and information engineering with the Department of Engineering, Universitã della Campania. His current research interests include electromagnetic inverse source problems, electromagnetic field sampling, and antenna diagnostics.

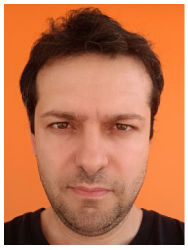

ANTONIO CUCCARO received the Laurea (summa cum laude) and Ph.D. degrees in electronic engineering from Seconda Universitã degli Studi di Napoli (SUN), Aversa, Italy, in 2012 and 2015, respectively. Then, he joined the Research Group in Applied Electromagnetic, SUN. Then, he was a Research Fellow with the University of Campania "Luigi Vanvitelli." He is currently a Researcher with the Department of Informatics, Modeling, Electronics and Systems Engineering (DIMES), Università della Calabria. His current research interests include through-the-wall imaging applications, biomedical imaging, and antenna design and diagnostics.

RAFFAELE SOLIMENE (Senior Member, IEEE) received the Laurea (summa cum laude) and Ph.D. degrees in electronic engineering from the Seconda Universitá degli Studi di Napoli (SUN), Aversa, Italy, in 1999 and 2003, respectively. In 2002, he became an Assistant Professor with the Faculty of Engineering, Mediterranea University of Reggio Calabria, Italy. Since 2006, he has been with the Dipartimento di Ingegneria, University of Campania "Luigi Vanvitelli," where he is currently a Full Professor. Based on the following topics, he has coauthored more than 250 scientific works. His research interests include inverse electromagnetic problems with applications to inverse source and array diagnostics, non-destructive subsurface investigations, through-the-wall and GPR imaging, and breast cancer detection. On these topics, he routinely serves as a reviewer for a number of journals, organized several scientific sessions, and edited a number of special issues. He is also an Associate Editor for four scientific journals, among which IEEE GEOSCIENCE AND REMOTE SENSING LETTERS.

Open Access funding provided by 'Università degli Studi della Campania "Luigi Vanvitelli"'
within the CRUI CARE Agreement